

Selection of flow-distributed oscillation and Turing patterns by boundary forcing in a linearly growing, oscillating medium

David G. Míguez,¹ Patrick McGraw,² Alberto P. Muñozuri,³ and Michael Menzinger²

¹*Department of Chemistry and Center for Complex Systems, MS015, Brandeis University, Waltham, Massachusetts 02454-9110, USA*

²*Department of Chemistry, University of Toronto, Toronto, Ontario, Canada M5S 3H6*

³*Grupo de Física Non Lineal, Universidade de Santiago de Compostela, A Coruña, 15782 Santiago de Compostela, Spain*

(Received 23 June 2008; published 20 August 2009)

We studied the response of a linearly growing domain of the oscillatory chemical chlorine dioxide-iodide-malonic acid (CDIMA) medium to periodic forcing at its growth boundary. The medium is Hopf-, as well as Turing-unstable and the system is convectively unstable. The results confirm numerical predictions that two distinct modes of pattern can be excited by controlling the driving frequency at the boundary, a flow-distributed-oscillation (FDO) mode of traveling waves at low values of the forcing frequency f , and a mode of stationary Turing patterns at high values of f . The wavelengths and phase velocities of the experimental patterns were compared quantitatively with results from dynamical simulations and with predictions from linear dispersion relations. The results for the FDO waves agreed well with these predictions, and obeyed the kinematic relations expected for phase waves with frequencies selected by the boundary driving frequency. Turing patterns were also generated within the predicted range of forcing frequencies, but these developed into two-dimensional structures which are not fully accounted for by the one-dimensional numerical and analytical models. The Turing patterns excited by boundary forcing persist when the forcing is removed, demonstrating the bistability of the unforced, constant size medium. Dynamical simulations at perturbation frequencies other than those of the experiments showed that in certain ranges of forcing frequency, FDO waves become unstable, breaking up into harmonic waves of different frequency and wavelength and phase velocity.

DOI: [10.1103/PhysRevE.80.026208](https://doi.org/10.1103/PhysRevE.80.026208)

PACS number(s): 05.45.-a, 82.40.Ck, 47.54.-r

I. INTRODUCTION

Oscillating media which are at rest and grow axially by addition at a growth boundary or which move in an open flow [1], and whose boundary conditions at the growth or inflow boundary are fixed or periodically forced, are known to develop stationary [2–4] and traveling waves [5–7], depending on the boundary-forcing frequency. Axially growing media and open flows are physically equivalent [5,6] since they are related by a Galilei transformation [8]. Both map the oscillatory dynamics of the medium onto space and the waves are called [3,5,7] flow-distributed oscillations (FDO).

FDO waves can exist under a much wider range of conditions than Turing patterns since they do not require differential transport. As a pattern-forming mechanism, they play a key role in the early development of higher organisms, whose common feature is a spatial domain that expands axially from a growth zone. This growth, combined with genetic oscillation of the medium (or, in biological terms, the existence of a “segmentation clock” [9]) and their eventual arrest play a key role in the transverse segmentation of developing embryos. They govern the formation of gene-expression waves that result in the formation of somites [5–7,10], the precursors of vertebrae and body segments [5,6,11]. In this view the size of somites is controlled by the linear growth rate divided by the initial oscillation frequency [5,6].

The properties of FDO waves (their wavelength and phase velocity) are determined, in the simplest approximation, by the phase kinematics of the oscillating medium [5–7], as discussed in Sec. VI. In the absence of strong gradients and of diffusion, each fluid element acts as an independent oscillator, with an initial phase set at the upstream boundary. In the

presence of diffusion, however, nearby fluid elements are coupled. This can result in damping and shifting of the oscillation frequency and in other effects. The essential kinematics remains however the same provided the intrinsic oscillation frequency is viewed as a variable that depends on the pattern wavelength. Differential transport introduces other complications, such as the possibility of Turing and differential flow (DIFI) instabilities. The concept of FDO was generalized to include differential flow and diffusion, in which case the resulting stationary waves are known as flow and diffusion-distributed structures (FDS) [12] which have been experimentally verified [13,14]. In the general case these compete with various types of traveling waves [15,16] that come into play when the system is perturbed by noise [16].

A linear stability analysis near an unstable homogeneous fixed point state is one way to predict the frequencies and wavelengths at which undamped stationary or traveling waves can occur, and which modes may be excited by an oscillating boundary condition. This is done by solving a dispersion relation for the appropriate wave ansatz [17,18]. Instabilities in a flow system or growing medium may be convective or absolute, depending on the relative rates of growth or flow v and of the intrinsic rate of spreading v_{sp} of a localized disturbance [19,20]. In the convective case, in which we are interested here, the growth (flow) rate is greater than the spreading velocity $v > v_{sp}$. Consequently a disturbance can only propagate away from the growth or inflow boundary [21], and therefore the inflow boundary condition controls the dynamics of convectively unstable systems and selects the global modes. This can lead to so-called “noise-sustained structures” if there is random noise at

the upstream boundary [20]. Here we consider a different situation where instead of noise there is a “signal” at the boundary that can select particular wave modes.

While analyzing convective instabilities of an unstable fixed point state with differential transport, it was found [18] that a quite generic behavior is for two sets of convectively growing modes to exist in different regions of boundary-forcing frequencies. FDO modes occur when the driving frequency is zero or comparable to the intrinsic oscillation frequency of the medium, while in the presence of differential diffusion, Turing modes can occur, generally at higher frequencies. The latter are essentially the standard Turing patterns, except that they are advected with the moving medium and their wavelengths can be selected by varying the boundary-forcing frequency. These predictions are borne out by nonlinear simulations [18].

Other complications, such as the nonlinear competition of different modes, depend on both diffusion and nonlinearity and therefore cannot be fully addressed either by linear stability analysis or by the kinematic picture. For example, FDO waves may become unstable [4], break up and reorganize into resonant waves [22] at a harmonically related frequency and a nonlinear boundary forcing may excite jumping waves [23], which at large downstream distances may ultimately be smoothed out or else break up into secondary waves.

The first objective of this paper is to verify experimentally the predictions [18] of two types of boundary-controlled waves (demonstrating the excitation and control of both FDO and Turing waves), that arise in a boundary-forced, growing, oscillating medium in the presence of strong differential diffusion. Previously, stationary and traveling FDO waves were demonstrated experimentally in a flow system without differential transport [24]. A medium that is Turing-as well as Hopf-unstable (in particular, the use of boundary forcing to select one or the other) represents a new ingredient in this context. Our second aim is to compare the experimental results qualitatively and quantitatively with analytical and numerical predictions and to clearly demonstrate that the kinematic nature of FDO waves persists, regardless whether differential transport is present or not.

In the remainder of this paper, we first describe our experiments and results, and then interpret the results with the aid of comparisons with numerical models and with the predictions of a linear analysis and an understanding based on phase kinematics.

II. EXPERIMENT

For the experiments the photosensitive chlorine-dioxide-iodide-malonic acid (CDIMA) reaction [25] was used in its oscillatory domain in a quasi-two-dimensional (quasi-2D) medium. To study its dynamics under conditions of pronounced differential diffusion, the system was tuned so that its fixed point was subject to both Hopf and Turing instabilities. The experiments were done in a one-side-fed unstirred reactor (CFUR) connected to a continuously fed stirred tank reactor (CSTR) [26,27]. The spatial structures were formed in a thin agarose gel (0.3 mm thick, 20 mm diameter, 2%

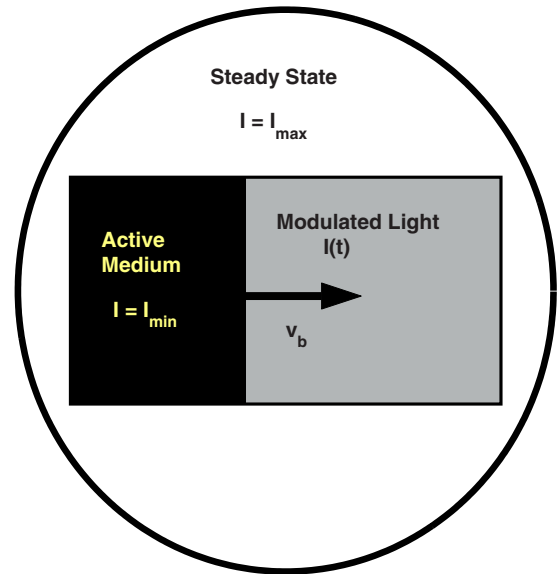


FIG. 1. (Color online) Schematic of the experimental setup. In the gray area to the right of the moving boundary, the medium is periodically forced by an oscillating light intensity. The black area, with minimal illumination, contains the actively oscillating medium where waves form. Outside the rectangle, all oscillations are suppressed by a large light intensity I_{\max} .

Agarose) separated from the CSTR by Anapore and nitrocellulose membranes. The CSTR was fed with a stream of the following composition: $[I_2]=0.6$ mM, $[MA]=1.2$ mM, $[ClO_2]=0.15$ mM, $[H_2SO_4]=10$ mM, $[PVA]=0.25$ g/l, where MA stands for malonic acid and PVA stands for polyvinyl alcohol. The CSTR residence time was 125 s and the reactor temperature was 4 ± 0.5 °C.

The photosensitivity of the CDIMA medium [28] was used to achieve both the growth of the active medium and its periodic boundary forcing. In the stationary medium there is no physical flow, hence differential flow is absent and only differential diffusion, arising from the partial immobilization of the activator, comes into play. The principle of the experiment is illustrated by Fig. 1. A computer-controlled data projector was used to cast the image shown onto the circular CDIMA medium [27,29]. The area outside the spatially fixed rectangular (black+gray) domains was inactivated by light of sufficiently high intensity I_{\max} . The black rectangular “active” domain received minimal, ambient light I_{\min} and it was made to grow with velocity v_b along its right edge into the gray domain. The latter area received a periodically modulated light flux $I(t)=I_0+I_1 \cos(\omega t)$, where $\omega = 2\pi f$, $I_0=10450 \pm 50 \times 10^{-6}$ W/cm², and $I_1=9350 \pm 50 \times 10^{-6}$ W/cm². Note that the midpoint I_0 of the modulated light flux was substantially higher than the intensity I_{\min} in the active domain—the light intensity oscillates between I_{\min} and I_{\max} . This implies that the boundary perturbation had a significant zero-frequency, dc component along with the oscillatory component. One unexpected consequence of this is the breakup and rearrangement of the waves at some driving frequencies into resonant waves of higher frequency and shorter wavelength. This will be briefly mentioned below and will be examined in detail in a subsequent paper. Images

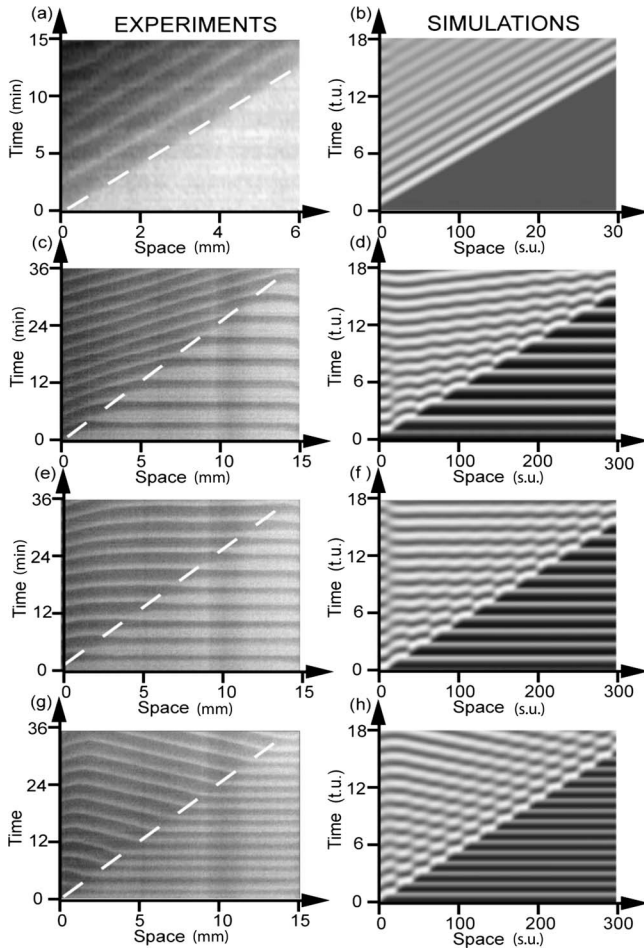


FIG. 2. Space-time plots of experimental (left column, panels a, c, e, and g) and numerically computed (right column, panels b, d, f, and h) at low perturbation frequencies $f/f_0 < 1.30$. The diagonal dashed lines represent the constant velocity v_b of the moving boundary. Forcing frequencies increase from top to bottom: a and b: $f/f_0=0.0$; c and d: $f/f_0=0.61$; e and f: 0.95; g and h: 1.30. The space and time units in the simulation plots are the dimensionless units of the model Eq. (1).

of the patterns evolving in the active domain were acquired by a charge-coupled device (CCD) camera that was connected to a computer for image enhancement and further analysis.

Typical experimental one-dimensional (1D)-space/time plots, generated from the two-dimensional (2D) image file by stacking the intensity profile along a suitably chosen line, parallel to the growth axis, are shown in the left-hand panels of Figs. 2 and 3. The diagonal dashed lines represent the moving boundary, whose velocity was within the range $v_b = 0.42 \pm 0.08$ mm/min in all experiments. The bottom-right half of the plots represents the periodically forced medium ahead of the expanding active domain, and it displays oscillations whose spacing is equal to the forcing period $T=1/f$. The FDO/FDS waves appear in the upper-left halves of the plots. Their vertical (temporal) spacing reflects the natural oscillation period of the reaction-diffusion system, and their phase velocities and wavelengths are constrained by simple geometrical (kinematic) considerations which are described in Sec. VI.

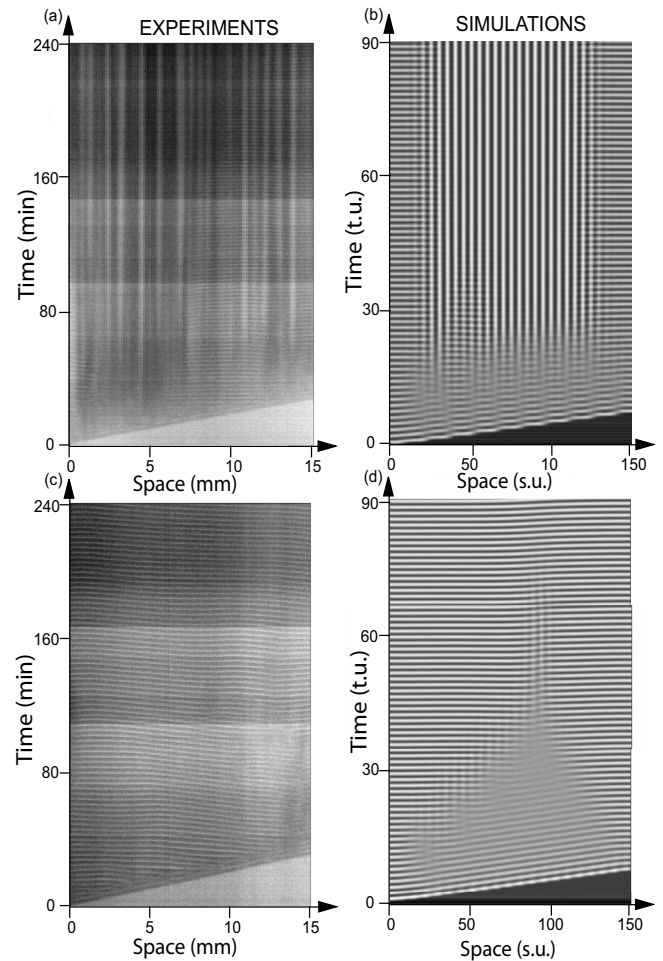


FIG. 3. Space-time plots similar to the ones in Fig. 2, measured (panels a and c) and computed (b and d) at high perturbation frequencies. a and b: $f/f_0=5.06$; c and d: $f/f_0=8.0$

The spreading velocity of a reaction-diffusion wave was measured as follows. Without illumination the circular CDIMA medium was allowed to oscillate. The rapid periodic phase waves [30] that sweep through the medium initially eventually slowed down through the intervention of diffusion [31], until, after 90 min they had reached their asymptotic reaction-diffusion velocity. Their spreading velocity was measured as $v_{sp} = 0.35 \pm 0.08$ mm/min from a space-time plot [21]. All experiments were performed in the convectively unstable regime $v_b \geq v_{sp}$ close to the absolute instability limit $v_b = v_{sp}$. Note that the system was tuned to lie close to its Hopf and Turing bifurcations as well as to its convective/absolute instability limit.

To test the response of the system to perturbations other than those of illumination at the moving boundary, a supplementary experiment was performed in which the growth velocity was modulated [22] at constant light intensity at the boundary, according to $v(t) = v_0 + v_1 \cos(\omega t)$. The velocity modulation $v_0 = v_1 = 0.42 \pm 0.08$ mm/min was quite pronounced, i.e., the velocity varied from zero to 0.84 mm/min.

III. EXPERIMENTAL RESULTS

Figures 2 and 3 show the experimental space time plots in the left-hand panels and the corresponding simulation results

TABLE I. Measurements of FDO wave properties from experimental space-time plots.

$T(\text{min})=1/f$	$T_0(\text{min})=1/f_0$	v_b (mm/min)	$1/C$ (min/mm)	$T_0/T=f/f_0$	v_b/C
∞	2.37 ± 0.06	0.47 ± 0.01	2.97 ± 0.14	0	0.93 ± 0.04
4.49 ± 0.02	2.72 ± 0.03	0.399 ± 0.008	1.16 ± 0.08	0.61 ± 0.02	0.38 ± 0.03
3.51 ± 0.03	3.31 ± 0.02	0.410 ± 0.008	0.03 ± 0.05	0.95 ± 0.02	0.010 ± 0.015
2.42 ± 0.02	3.14 ± 0.02	0.415 ± 0.005	-1.00 ± 0.06	1.30 ± 0.02	-0.33 ± 0.02

in the right-hand panels, at six values of the forcing frequencies that increase from top to bottom. The simulation model is described in the next section. Experimental data of the frequencies and velocities, derived from direct measurements on the space-time plots, are collected in Table I. The phase velocity and frequency of the FDO waves were measured directly from the space-time plots. Since the phase velocity diverges for the waves driven near the natural oscillation frequency, we recorded the inverse phase velocities $1/C$ rather than C . For similar reasons, the wavelengths are not reported in Table I. To facilitate comparisons between the experimental results and numerical and analytical predictions, all forcing frequencies were normalized by the measured oscillation frequency of the (unstirred) reaction-diffusion system, and numerical simulations were done at similar values of this ratio. The values compared, in other words, are those of $f/f_0=T_0/T=1/R$, where T_0 was measured separately for each experiment.¹ The reduced frequencies lie in the range $0 \leq f/f_0 < 8$.

At constant forcing $f/f_0=0$ the wave train shown in panel 2(a) moves at the same rate as the boundary (it is stationary in the comoving frame of the equivalent flow system [2,3,7]). Note that the amplitude of the waves decays slightly with increasing distance from the boundary. This decay will be shown to be consistent with linear dispersion analysis. A longer simulation reveals them to be transient waves, and we expect that an experiment run for a longer time would also show that the waves produced by constant forcing eventually decay to nothing. At slow forcing $f/f_0=0.61$ periodic waves move in the same direction as, and faster than (i.e., toward) the moving boundary, $C > v$, as shown in panel 2(c). Panel 2(e), obtained with forcing near the natural frequency of the RD system, $f/f_0=0.95$, shows almost homogeneous bulk oscillations or waves with nearly infinite velocity and infinite wavelength near the moving boundary. In panel 2(g), obtained at $f/f_0=1.30$, the dominant waves move away from the moving boundary. The direction of the dominant waves agrees in all cases with that predicted for flow systems [5,7,18] if the change of reference frame is taken into account (see Sec. VI). Near the fixed (left-hand) boundary, however, the waves in panels 2(e) and 2(g) propagate in the

direction opposite to those near the moving boundary, suggesting an influence of the fixed boundary within a boundary layer.

The results obtained at high forcing frequencies are given in Fig. 3. Figure 3(a) shows a series of irregularly spaced stationary waves that grow slowly with time and reach their full amplitude long after the boundary has moved out of the system, which no longer grows at this time. The snapshot of the 2D structure shown in Fig. 4, from which Fig. 3(a) was constructed, identifies the stationary waves as Turing spots. These nascent hexagonal spots exhibit typical irregularities which would anneal only after many hours [32].

While the excitation of the Turing mode at high perturbation frequency is expected from both the dispersion relation and the 1D simulations in this region of parameter space [18], the two-dimensional nature of the experimental medium apparently has a radical effect on the nature of the Turing patterns. The 1D simulations show a clear selection of the wavelength by the boundary-forcing frequency, namely, $\lambda=v_b T$ where T is the forcing period, but the patterns appearing in the experimental results are manifestly not

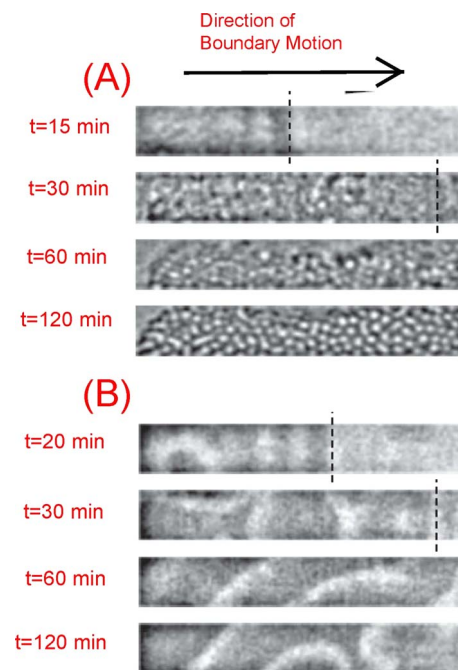


FIG. 4. (Color online) Series of 2D snapshots of the system forced at high frequencies. The length of the region shown here is 37.5 mm. (a) $f/f_0=5.0 \pm 0.6$ (within the window where Turing patterns are expected) and (b) $f/f_0=8.0 \pm 0.9$ (above the Turing window). The dotted lines show the position of the moving boundary.

¹For the two experiments with higher driving frequencies $f/f_0=5.0, 8.0$, there were no sustained coherent self-oscillations to measure, as Turing or other structures were formed instead. In these cases, the natural period T_0 was taken to be the average of periods measured in the other experiments, with uncertainty corresponding to the deviation of those values. Variations in the natural frequency and their significance will be discussed further in Sec. VI.

quasi-one-dimensional and it is much less clear how (or if) their spacing is controlled by the boundary forcing.

Figures 3(c) and 3(d) show that at an even higher perturbation frequency $f/f_0=8.0$, neither FDO nor Turing structures are excited. This is consistent with results from linear dispersion analysis, see below. In the simulation (Fig. 3) in the top panel of Fig. 4(a) there is a rapidly decaying wave, just behind the moving boundary. It appears to be a transient, damped FDO wave moving at the same speed as the boundary like the one found at $f/f_0=0$ and is presumably due to the zero-frequency component of the driving signal that was mentioned previously.

We remark that the Turing structures which are formed at $f/f_0=5.0$ reach their full amplitude and persist long after the boundary has reached the end of the active rectangle and stopped moving, just as the FDO waves are sustained long after the boundary has passed. This highlights the multistability of the medium, and the corresponding multiple instability of the homogeneous fixed point state. FDO waves and Turing patterns are competing patterns supported by the medium. The essential aspect of the FDO mechanism (or, in this case, the FDO mechanism extended to include strong differential diffusion and Turing structures) is that the boundary plays a role in determining which of the competing patterns begin to be established—once established they may persist long after the driving signal that gave rise to them has ceased to exist. Analogously in the case of a flow system with a fixed upstream boundary, the driving of the upstream boundary imposes a structure that can be advected along with the fluid and sustains itself after the advected fluid has long since lost diffusive contact with the boundary.

The supplementary experiment, in which the growing medium was perturbed by modulating the growth rate [22] instead of the illumination, gave results that were qualitatively similar to those in Figs. 2 and 3 at similar perturbation frequencies $f/f_0=0.93;8.0$. Apparently, modulation of boundary condition and of growth rate may be used interchangeably for mode selection. This is closely analogous to results found previously in numerical simulations of a flowing system with fixed boundary [22], where it was shown that modulation of the flow velocity could lead to the breakup of a transient stationary wave to form traveling FDO waves with frequencies selected by the velocity modulation frequency [33–40].

IV. NUMERICAL SIMULATIONS

To simulate our experimental system numerically, we used the Lengyel-Epstein kinetic model [25] of the CDIMA reaction. In dimensionless form for one spatial dimension, the model is given by the following equations:

$$\begin{aligned}\partial_t u &= a - bu - \frac{4uv}{1+u^2} - \phi(t) + d\partial_x^2 u, \\ \partial_t v &= \sigma \left(bu - \frac{uv}{1+u^2} + \phi(t) + d\partial_x^2 v \right),\end{aligned}\quad (1)$$

u and v are the dimensionless concentrations of activator and inhibitor and a , b , and σ are control variables and rate con-

stants. The effective ratio of diffusion coefficients that arises from partial immobilization of the activator, is $d\sigma$. ϕ is related to the light intensity; the ϕ terms represent the photosensitivity and account for the growth of the active domain and the modulation of the boundary by light. On the illuminated side of the moving boundary $x > v_b t$ the light intensity in the simulations is $\phi(t) = \phi_0 + \phi_1 \cos \omega t$ and it is $\phi_{\min} = 2.0$ on its dark side $x > v_b t$.

The following set of parameters was chosen to mimic approximately the dynamics of the experimental system: $a = 22$, $b = 1.3$, $d = 1.07$, $\sigma = 8.5$, with moving-boundary velocity $v_b = 20$ s.u./t.u. The forcing parameters are $\phi_0 = 3$, $\phi_1 = 1$. The equations were solved using an explicit second-order method. Space and time steps were $\Delta x = 0.1$ and $\Delta t = 2.0 \times 10^{-4}$.

The simulation results are shown in the right-hand panels Figs. 2(b), 2(d), 2(f), and 2(h) and in Figs. 3(b) and 3(d) for the same values of the frequency ratio as the experiments. These and further simulations will be fully analyzed in the dimensionless plots, Fig. 7, as described in Sec. VI. The qualitative agreement with experiments is good: the waves travel in the same direction and panel (h) also shows the reversal of propagation direction near the fixed (left-hand) boundary, similar to that observed in panel (g). The pulsations of the waves behind the moving boundary in Figs. 3(d), 3(f), and 3(h) resemble those of recently calculated FDO waves that were perturbed by a sinusoidally modulated flow [22]. When the perturbation frequency was an integer fraction of the natural oscillation frequency, it was found that the flow-modulated waves could become unstable and lead to the resonant breakup and reconnection of the wave trains. The pulsations are also analogous to those of “jumping” waves excited by a boundary driving signal which is different from the natural limit cycle of the oscillating medium, observed in both simulations and experiments with flow systems [23]. In the present experiments, however, these modulations are not noticeable, suggesting that the quasi-2D medium acts as a kind of buffer that smoothes the pulsations found in the 1D model system.

The simulation and experiment at high driving frequencies shown in Figs. 3(a) and 3(b) show both similarities and dissimilarities. In both cases, stationary Turing waves continue to grow slowly out of the background, once the moving boundary has passed the system. In the numerical calculations, they are regular and periodic, with wave number proportional to the driving frequency, as expected. The experimental Turing pattern, on the other hand, is two-dimensional and irregular as noted in the previous section. Another difference between the simulations and the experimental results is evident in the behavior near the fixed boundaries (the left boundary is always fixed, and the moving right boundary eventually stops moving and becomes a fixed one after the active domain has reached its maximum length.) In the simulation, unlike the experiment, there is a well-defined boundary layer near each of these fixed boundaries. These boundary layers exhibit Hopf oscillations rather than Turing patterns. In the case of Fig. 3(b), there is a stationary boundary between the oscillating boundary layer and the Turing patterns. In Fig. 3(d), however, no patterns are excited by the moving boundary except for the decaying transient FDO

waves. These transient waves are presumably excited by the zero-frequency component of the boundary condition, and they decay as predicted by the linear dispersion relation (see next section). In the case of the simulations, these transient waves decay to a uniform fixed point state, which is subsequently invaded by the Hopf oscillations that originate near the fixed boundaries. The experiment shows a slightly different behavior: the decaying waves near the moving boundary give way almost immediately to irregular oscillations that are not coherently synchronized across the length of the medium. One can be seen from the two-dimensional snapshot in Fig. 4(b) that these oscillations are actually two-dimensional patterns that are not evidently aligned with the boundary.

V. LINEAR DISPERSION RELATIONS

As shown elsewhere [18,41], linear stability analysis of the governing Eqs. (1) around the fixed point of the local system leads to a dispersion relation for wavelike disturbances that is quartic in the complex wave number k . To derive the dispersion relation for waves driven by a boundary condition driven with steady amplitude, one should use the reaction-diffusion-advection equations in the frame of reference of the equivalent flow system with a fixed boundary [17,18]. Issues of the choice of reference frames will be discussed in the following paper. The flow system is described by

$$\begin{aligned} \partial_t u &= a - bu - \frac{4uv}{1+u^2} - \phi(t) + \partial_x^2 u - v_b \partial_x u \\ &= f(u, v, t) + D_u \partial_x^2 u - v_b \partial_x u, \\ \partial_t v &= \sigma \left(bu - \frac{uv}{1+u^2} + \phi(t) + d \partial_x^2 v \right) - v_b \partial_x v \\ &= g(u, v, t) + D_v \partial_x^2 v - v_b \partial_x v, \end{aligned} \quad (2)$$

where $D_u=1$ and $D_v=\sigma d$

Dispersion relations are obtained by considering a small perturbation of the fixed point, of the form

$$\begin{pmatrix} u \\ v \end{pmatrix} = \begin{pmatrix} u_0 \\ v_0 \end{pmatrix} + \begin{pmatrix} U \\ V \end{pmatrix} \exp i(\omega t - kx), \quad (3)$$

where the fixed point (u_0, v_0) under constant illumination ϕ is given by

$$u_0 = \frac{a - 5\phi}{5b}, \quad v_0 = a \frac{1 + u_0^2}{5u_0}$$

and (U, V) are the perturbation amplitudes. Here, ω is taken to be a purely real frequency, assuming that the system is driven with a steady amplitude. The wave number k is in general complex as the wave may grow or decay with increasing distance from the inflow boundary. $\text{Re } k$ and $\text{Im } k$ are the wave number and spatial growth rate, respectively. (In general U and V may also be complex—see [18]). Substitution of the ansatz [Eq. (3)] into the Eqs. (2) leads to the dispersion relation

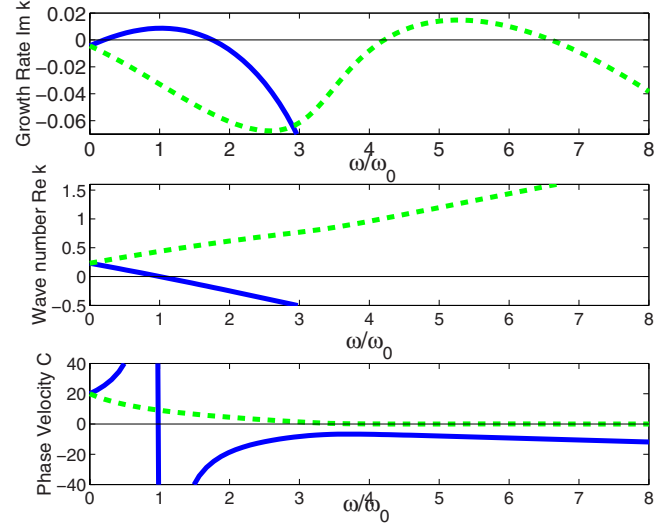


FIG. 5. (Color online) Solutions of dispersion relations for small-amplitude waves based on linear stability analysis of the unstable fixed point state. The two solutions each reach a peak growth rate in a different band of frequencies. The lower frequency peak in the solid curve represents FDO modes, and the other peak contains Turing modes. At the natural oscillation frequency, the corresponding FDO modes have zero wave number and infinite phase velocity. The Turing modes, on the other hand, have zero phase velocity.

$$\begin{aligned} 0 &= (v_b k - \omega)^2 + i[k^2(D_u + D_v) - \text{Tr } \mathbf{J}](v_b k - \omega) \\ &\quad + k^2(D_u J_{uu} + D_v J_{vv}) - k^4 D_u D_v - \det \mathbf{J}, \end{aligned} \quad (4)$$

where

$$\mathbf{J} = \begin{pmatrix} \frac{\partial f}{\partial u} & \frac{\partial f}{\partial v} \\ \frac{\partial g}{\partial u} & \frac{\partial g}{\partial v} \end{pmatrix} \Bigg|_{(u_0, v_0)} \quad (5)$$

is the Jacobian matrix of the chemical kinetic equations evaluated at the fixed point. Since the dispersion relation is quartic in k , there are four solutions for $k(\omega)$ —two pairs of complex conjugate mirror images. Two of them are physically relevant near the growth (or inflow) boundary, and the other pair is associated with the fixed (or downstream) boundary [18]. The real parts $\text{Re}(k)$ of the eigenvalues are the wave number and the imaginary parts $\text{Im}(k)$ are the growth rates. The phase velocity in the flow system is given by $c = \omega / \text{Re } k$. In the equivalent growing system the phase velocity is Galilei-transformed to $C = v_b - c$. Figure 5 shows plots of $\text{Re } k$, $\text{Im } k$, and C for both relevant solutions as functions of f/f_0 , obtained by numerically solving the dispersion relation (4). The frequency $f_0 = 0.7613 \text{ t.u.}^{-1}$ was obtained from a simulation of the reaction-diffusion system. As before [18], Fig. 5 reflects two modes with locally positive growth rates. One solution branch (the solid curve in the figure) has positive growth rate for frequencies $0.20 < f/f_0 < 1.75$. These modes correspond to FDO waves. The phase velocity of these waves has a pole at $f/f_0 \approx 1$, as

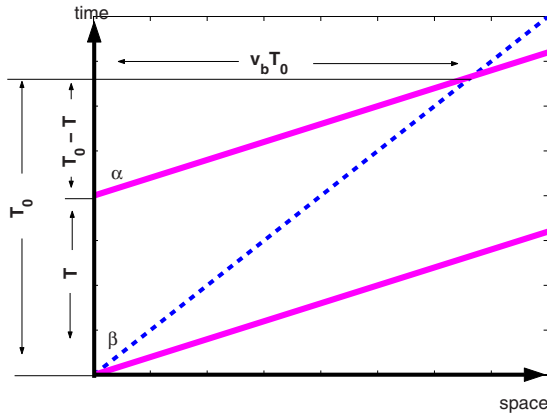


FIG. 6. (Color online) Illustration of phase kinematics of FDO waves. Dotted line: trajectory of a point moving with the fluid flow. Solid lines: two successive phase fronts or wave crests.

expected from phase kinematics.² At zero frequency, $C = v_b = 20$ t.u./s.u., or in other words the waves produced by zero-frequency forcing move at the same speed as the boundary. Note however, that the zero-frequency waves are slightly damped. This is consistent with the simulation and experimental results, in which these zero-frequency waves appear to be decaying slightly with increasing distance from the boundary. FDO waves also become damped for frequencies $f/f_0 > 1.75$. The other solution shows a positive growth rate in the higher frequency interval $4.2 < f/f_0 < 6.6$. These growing modes correspond to Turing patterns. As expected for Turing patterns, they have vanishing phase velocity C , i.e., they are stationary with respect to the medium. The two peaks are separated by a gap of decaying modes at $1.75 \lesssim f/f_0 \lesssim 4.2$. No experimental points were collected in this gap, but nonlinear simulations at these frequencies show unexpected results which will be analyzed in the following paper.

VI. PHASE KINEMATICS OF WAVES

This section summarizes the kinematics of phase waves that arise in boundary-forced (at frequency f) self-oscillating media (with intrinsic frequency f_0), which either flow or grow with velocity v_b . The basic kinematic relationships of these waves can be derived in several different ways [5,6]. Here, we read them straightforwardly from the geometry of a space-time diagram. We derive them first for a flowing medium and then apply the Galilean transformation to the equivalent moving-boundary system. Figure 6 illustrates schematically the space-time plot for phase waves in a flowing, self-oscillating medium. Two successive phase fronts (wave crests) are shown, traveling with velocity $c = \tan \alpha$. The worldline of an arbitrary point advected with the fluid

flow is also shown, with velocity $v = \tan \beta$. The vertical distance between two successive wave crests is by definition T , the period of the traveling wave. On the other hand, if the wave behavior is due to the self-oscillation of the medium and a point advected along with the fluid flow is assumed to be oscillating at the intrinsic frequency f_0 , then its trajectory must intersect the two successive wave crests at times separated by one oscillation period $T_0 = 1/f_0$. (Note that what we call the intrinsic frequency need not be identical to the batch-mode oscillation frequency [24]—see below) During this time the distance traveled by the advected reference point is $v_b T_0$. From the diagram, it is then readily apparent that a phase front travels the same distance $v_b T_0$ in time $T_0 - T$, and hence the phase velocity of the waves is

$$c = \tan \alpha = \frac{v_b T_0}{T_0 - T} = \frac{v_b}{1 - R}, \quad (6)$$

where $R \equiv f_0/f = T/T_0$. The wavelength of the phase waves is then given by

$$\lambda = cT. \quad (7)$$

Note that in the case $f < f_0$, the derivation works the same way, but in this case the phase velocity becomes negative, i.e., the wave fronts move upstream. The case $T = T_0$ represents a uniform, synchronized oscillation of the whole system. In this case, the phase velocity and wavelength are infinite. When the medium is growing and stationary, as in developing organisms, the velocity C relative to the medium is obtained by subtracting the growth rate

$$C = v_b - c = v_b \frac{1}{1 - \frac{T_0}{T}}. \quad (8)$$

The sign reversal is necessary if the flow velocity in the flow system and the boundary velocity in the growing system are both taken to be positive.

The frequency of the waves as measured in the moving-boundary frame is f_0 , since a point advected with the fluid in the flow system is equivalent to a stationary point in the moving-boundary frame. In the normal case of waves controlled by the driving at the boundary, the frequency of waves in the flow system is equal to the forcing frequency. The above derivations are purely kinematic or geometric. In the simplest case, called the “kinematic limit,” the “intrinsic” period T_0 is a constant and is the same as the natural limit cycle period of the underlying chemical oscillator. Stronger diffusion, however, can couple the oscillations of nearby fluid elements and alter their dynamics, possibly changing the oscillation period. Diffusion is unimportant when there are very weak gradients, which is the case for the nearly synchronous oscillations that occur near $T \approx T_0$. Deviations from the kinematic limit occur when both strong diffusion and large gradients exist. Since the above relationships were derived purely geometrically, they remain valid away from the kinematic limit provided one defines T_0 as variable rather than constant. This variable effective T_0 depends on the diffusion constants, the wavelength of the wave and thus implicitly on the frequency. In the frame of reference where the

²The pole is actually shifted slightly from $f/f_0 = 1$. This is because small-amplitude oscillations have a slightly different frequency from the stable limit cycle. The dispersion relation for small-amplitude waves reflects the former, whereas the normalization constant f_0 is the frequency of large-amplitude oscillations.

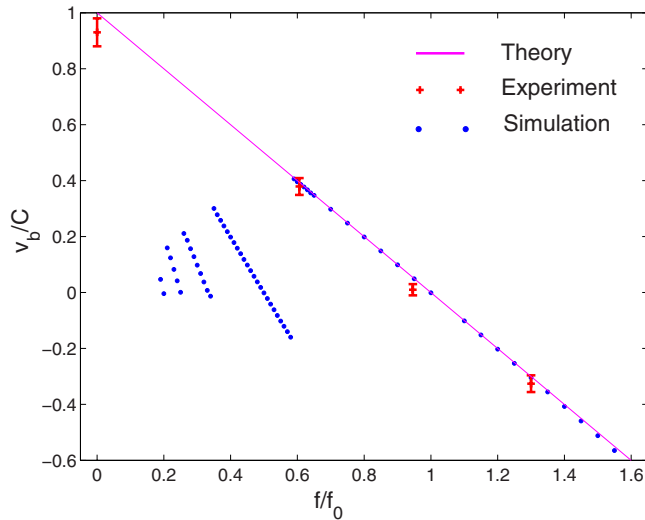


FIG. 7. (Color online) Kinematic relations of FDO wave properties for experimental and numerical results. For smoothly propagating phase waves driven by the boundary driving frequency, all data should fall on the indicated straight line. The numerical results which fall off of this line at frequencies $0.2 \lesssim f/f_0 \lesssim 0.6$ represent harmonic resonances, as mentioned in the text.

medium is stationary and growing, T_0 is the period of the waves as measured at a constant position. Numerical results discussed below lead us to expect that variations in T_0 attributable to these effects are too small to be detectable by the current experiment.

We can now analyze the kinematics of the FDO waves obtained numerically and experimentally. According to a rewritten version $v_b/C = 1 - f/f_0$ of Eq. (8), a plot of v_b/C vs f/f_0 should be linear provided that there are smoothly propagating phase waves controlled by the driving frequency according to the FDO mechanism. Figure 7 shows such a linear behavior for both the experimental and numerical results (with the exception of the numerical results for frequencies $0.2 \lesssim f/f_0 \lesssim 0.6$, which will be discussed in the following publication). The experimental phase velocity data are based on measurements of the space-time plots displayed in Fig. 2 (see Table I).

As for variations in the intrinsic oscillation frequency f_0 , the values of f_0 obtained from numerical and experimental results are plotted in Fig. 8. The numerical values vary by less than 1%, with the maximum occurring for synchronous oscillations $f/f_0=1$. The experimental values, on the other hand, vary by somewhat more than 10% from their average, and there is less of a clear systematic trend. This suggests that the variations in the experiments may largely be due to slight variations in experimental conditions, and therefore the current experiment is not sensitive to the very small shifts in the intrinsic frequency that arise from diffusion effects alone.

Turing waves controlled by the boundary also have properties determined by geometry and kinematics. They are stationary with respect to the medium. The boundary can be thought of as laying down successive stripes as it moves along. If each oscillation of the boundary deposits one Turing stripe, then the wavelength of the resulting pattern is

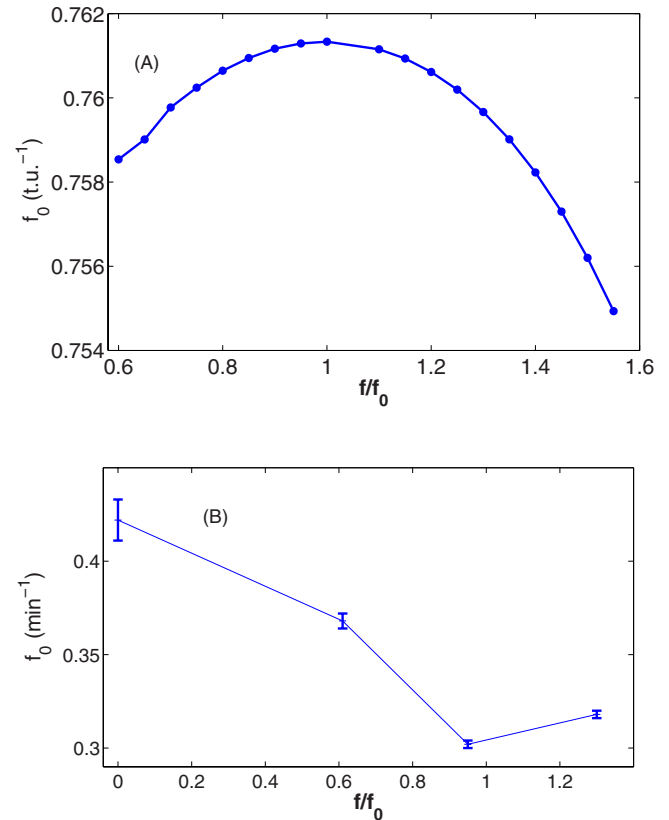


FIG. 8. (Color online) Variations in the (a) numerically and (b) experimentally measured intrinsic oscillation frequency f_0 , namely, the frequency measured at a stationary position in the domain of propagating FDO waves. Variations in the numerical values reflect only the small effects of diffusion within waves of different wavelengths.

directly proportional to the driving period via the boundary velocity: $\lambda = vT$. The boundary driving can produce Turing structures if the driving period is such that the resulting wavelength falls within the range of wavelengths against which the medium is Turing-unstable. Formally, boundary-controlled Turing structures can be treated within the same kinematic framework as above, provided one assumes an intrinsic frequency of zero for these patterns. In that case, the formulas given above [Eqs. (6)–(8)] give $c = v_b$, $C = 0$, and $\lambda = v_b T$.

VII. CONCLUSIONS

We have given an experimental demonstration of the excitation of traveling wave patterns in a growing stationary medium, with wave frequencies and types selected by means of forcing at the boundary. The experiments described here are complementary to the previous demonstration of stationary and traveling FDO waves in a flow system [24]. While a flow system and a growing system are equivalent in principle, they are realized differently in the laboratory. The current experiments introduced an additional new ingredient, differential diffusion, which was not present in the previous flow-system experiments. In the presence of strong differential diffusion, we verified the prediction that both FDO and

Turing modes can be selected by boundary forcing at different frequencies. Turing modes occurred as expected for higher forcing frequencies while FDO modes based on the intrinsic chemical oscillator were found at lower frequencies. The qualitative behavior of the FDO waves in terms of their phase velocities, wavelengths, and frequencies, was close to what was expected. Although the FDO and Turing patterns occurred within the predicted frequency bands, the Turing patterns that appeared in the experiments were two-dimensional and could not be fully accounted for by the one-dimensional models on which the predictions were based.

It is worth noting that in the experiments the forcing at the boundary was far from a simple harmonic, small perturbation of the unstable fixed point such as envisioned in deriving the dispersion relation, nor was it, as in previous flow-system experiments [24], closely related to the limit cycle of the chemical oscillator. Also, since the average illumination to the right of the moving boundary was much higher than in the active medium, the driving signal always contained a strong zero-frequency component as well as an oscillatory one. The selection of particular patterns thus occurred under

more complex conditions than the theoretical models that predicted them.

In the following paper we will discuss the anomalous results (see, for example, Fig. 7) that occurred in numerical simulations at frequencies other than the experimental ones (in particular, for low but nonzero frequencies and for frequencies in the expected gap between the FDO and Turing modes). It will also be worthwhile to examine further the impact of the two-dimensional medium on the formation of boundary-driven waves, as hinted at by the experimental Turing results. Previous experimental and numerical results [29] for absolutely (rather than convectively) unstable two-dimensional growing media showed a complicated dependence of Turing pattern orientation on the boundary velocity, and similar effects beyond the scope of one-dimensional modeling may be at work here.

ACKNOWLEDGMENTS

This work was supported by the DGI (Spain) under Project No. BFM2000-0348 and Xunta de Galicia (Spain) under Project No. PGIDT00PX120610PR and by the NSERC of Canada.

-
- [1] An open flow is characterized by an inflow and a corresponding boundary condition.
- [2] S. P. Kuznetsov, E. Mosekilde, G. Dewel, and P. Borckmanns, *J. Chem. Phys.* **106**, 7609 (1997); P. Andrésen, M. Bache, E. Mosekilde, G. Dewel, and P. Borckmanns, *Phys. Rev. E* **60**, 297 (1999).
- [3] M. Kærn and M. Menzinger, *Phys. Rev. E* **60**, R3471 (1999).
- [4] J. R. Bamforth, S. Kalliadasis, J. H. Merkin, and S. K. Scott, *Phys. Chem. Chem. Phys.* **2**, 4013 (2000); J. R. Bamforth, J. H. Merkin, S. K. Scott, R. Toth, and V. Gaspar, *ibid.* **3**, 1435 (2001).
- [5] M. Kærn, M. Menzinger, and A. Hunding, *J. Theor. Biol.* **207**, 473 (2000).
- [6] M. Kærn, M. Menzinger, R. Satnoianu, and A. Hunding, *Faraday Discuss.* **120**, 295 (2002).
- [7] M. Kærn, D. G. Miguez, A. P. Munuzuri, and M. Menzinger, *Biophys. Chem.* **110**, 231 (2004).
- [8] An open flow is related to an axially growing system by a Galilei transformation: the inflow is fixed and the medium flows in the former case, while in the latter, the growth boundary moves and the medium is fixed [5,6].
- [9] F. Giudicelli and J. Lewis, *Curr. Opin. Genet. Dev.* **14**, 407 (2004).
- [10] Y. Bessho and R. Kageyama, *Curr. Opin. Genet. Dev.* **13**, 379 (2003).
- [11] The somite size predicted from FDO agrees quantitatively with that in chick embryos [5,6].
- [12] R. A. Satnoianu and M. Menzinger, *Phys. Rev. E* **62**, 113 (2000); R. Satnoianu, P. K. Maini, and M. Menzinger, *Physica D* **160**, 79 (2001).
- [13] D. D. Miguez, R. A. Satnoianu, and A. P. Munuzuri, *Phys. Rev. E* **73**, 025201(R) (2006).
- [14] D. G. Miguez, G. G. Izus, and A. P. Munuzuri, *Phys. Rev. E* **73**, 016207 (2006).
- [15] P. V. Kuptsov and R. A. Satnoianu, *Phys. Rev. E* **71**, 015204(R) (2005).
- [16] P. V. Kuptsov, *Physica D* **197**, 174 (2004).
- [17] P. N. McGraw and M. Menzinger, *Phys. Rev. E* **68**, 066122 (2003).
- [18] P. N. McGraw and M. Menzinger, *Phys. Rev. E* **72**, 026210 (2005).
- [19] R. J. Briggs, *Electron Stream Interactions with Plasmas* (MIT, Cambridge, MA, 1964).
- [20] R. J. Deissler, *J. Stat. Phys.* **40**, 371 (1985); **54**, 1459 (1989).
- [21] In convectively unstable flows, perturbations are eventually washed out of a finite domain, while in an equivalent, growing, and stationary medium they grow in both directions.
- [22] P. N. McGraw and M. Menzinger, *Phys. Rev. E* **72**, 027202 (2005).
- [23] M. Kaern and M. Menzinger, *Phys. Rev. E* **61**, 3334 (2000).
- [24] M. Kærn and M. Menzinger, *J. Phys. Chem. A* **106**, 4897 (2002).
- [25] I. Lengyel, G. Rabai, and I. R. Epstein, *J. Am. Chem. Soc.* **112**, 9104 (1990).
- [26] A. K. Horvath, M. Dolnik, A. P. Munuzuri, A. M. Zhabotinsky, and I. R. Epstein, *Phys. Rev. Lett.* **83**, 2950 (1999).
- [27] D. G. Miguez, Ph.D. thesis, Universidad de Santiago de Compostela, 2005.
- [28] A. P. Munuzuri, M. Dolnik, A. M. Zhabotinsky, and I. R. Epstein, *J. Am. Chem. Soc.* **121**, 8065 (1999).
- [29] D. G. Miguez, M. Dolnik, A. P. Munuzuri, and L. Kramer, *Phys. Rev. Lett.* **96**, 048304 (2006).
- [30] N. Kopell and L. N. Howard, *Science* **180**, 1171 (1973).
- [31] S. Y. Su, R. L. Armstrong, M. Menzinger, A. Cross, and C.

- Lemaire, J. *Phys. Chem.* **98**, 2494 (1994).
- [32] Q. Ouyang and H. L. Swinney, *Nature (London)* **352**, 610 (1991).
- [33] A. M. Turing, *Philos. Trans. R. Soc. London, Ser. B* **237**, 37 (1952).
- [34] A. B. Rovinsky and M. Menzinger, *Phys. Rev. Lett.* **69**, 1193 (1992).
- [35] M. R. E. Proctor, S. M. Tobias, and E. Knobloch, *Physica D* **145**, 191 (2000).
- [36] J. R. Bamforth, R. Toth, V. Gaspar, and S. K. Scott, *Phys. Chem. Chem. Phys.* **4**, 1299 (2002).
- [37] R. Toth, A. Papp, V. Gaspar, J. H. Merkin, S. K. Scott, and A. F. Taylor, *Phys. Chem. Chem. Phys.* **3**, 957 (2001).
- [38] M. Kaern, R. Satnoianu, A. Munuzuri, and M. Menzinger, *Phys. Chem. Chem. Phys.* **4**, 1315 (2002).
- [39] P. Andrésen, E. Mosekilde, G. Dewel, and P. Borckmans, *Phys. Rev. E* **62**, 2992 (2000).
- [40] M. Kærn and M. Menzinger, *Phys. Rev. E* **62**, 2994 (2000).
- [41] R. A. Satnoianu, *Phys. Rev. E* **68**, 032101 (2003).